UWB Geo-Regioning - Algorithm and Performance

Frank Althaus, Christoph Steiner and Armin Wittneben
Communication Technology Laboratory, ETHZ, CH-8092 Zuerich
Email: {althaus, steinech, wittneben}@nari.ee.ethz.ch

***Abstract*— Geo-regioning is an approach to localize Ultra-Wideband transmitters by means of their signatures. Recently, the principle feasibility of this approach has been shown and a first geo-regioning algorithm was presented [1], [2]. In this paper we derive the optimum receiver for the underlying Gaussian assumption and we show that our initial algorithm performs almost optimal. We discuss the pairwise error performance deciding between two regions and show the impact of the number of available samples. We derive an approximation for the pairwise error probability which allows to investigate the impact of many performance parameters more easily and profoundly.**

I. Introduction

To motivate our approach we point out that one of the most cited advantages of Ultra-Wideband (UWB) technology is the capability of performing accurate localization [3]. The huge bandwidth introduces a very high temporal multipath resolution to the propagation channel including an accurate representation of the initial delay. Therefore, most localization and ranging approaches in UWB are based on *Time-of-Arrival* (ToA) estimation [4].
In [1], [2] the authors present a different approach exploiting the nature of UWB channels to achieve a rough localization for some specific applications. There, we suppose that the channel impulse response (CIR) of a transmitter/receiver (TX/RX) pair is almost unique, given by many resolvable multipath components that result from the individual geographical constellation of RX and TX. At a certain RX position the CIR received from any TX is like a signature of the TX's position. If two TXs have a very similar signature they are likely very close together. We refer to this approach as "geo-regioning".

In *data aided geo-regioning* the position of some specific reference nodes in the network is known. This information is used to derive the position location information of all received signals by means of an appropriate regioning process. This facilitates a variety of location aware services and protocols in dense ad hoc networks. In our geo-regioning approach we will only consider signatures without ToA information. Compared to ToA based techniques, for the geo-regioning approach much lower timing and synchronization accuracy is sufficient. Furthermore, there is no special protocol required for the transmitters to be localized as it is, e.g., for ranging [5]. This makes geo-regioning particularly appropriate for asynchronous networks. Since geo-regioning requires only estimates of the signatures at the receiver, heterogeneous types of UWB transmitters as, e.g., sensors, tags or communication devices can be localized. Although the performance of such a system can be increased using several receivers at different positions (as it is usual in localization systems [6][7]), only one single antenna receiver is sufficient for geo-regioning. Additionally, geo-regioning is a promising approach for localization in environments where no direct path can be received.

Our initial geo-regioning algorithm uses the knowledge of the average power delay profiles of the different regions. It could be shown that this is sufficient to perform the regioning decision with reasonable reliability. It is obvious that the feasibility and performance of geo-regioning depend very much on characteristics of propagation channel and environment and require rich multipath conditions. Therefore, a measurement campaign has been performed which provides an appropriate set of data to investigate geo-regioning by means of measured data [8].

The paper is organized as follows. We summarize the measurement campaign in Section II. We derive and compare two geo-regioning algorithms with different complexity in Section III. In Section IV we discuss performance results based on simulations with the measured data. In Section V we derive an approximation for the pairwise error probability which enables a more thorough investigation of the performance. Conclusions are given in Section VI.

II. Measurements

A time-domain measurement setup using correlation method is used. In each of the 22 measured regions in a warehouse like scenario more that 600 channel impulse responses have been collected where the position of the transmit antenna has been moved randomly. The spacing of these positions is roughly 1.7cm. Fig. 1 shows a floor plan of the room including some details on the furniture with the positions of the regions and the position of the receive antenna. Due to the chosen position of the RX antenna we have typical LOS regions from Region 1 to 11 and in Region 13 and 14. Typical NLOS region are 16 to 21.

Fig. 2 depicts 150 signatures measured in Region 13. A section of 20ns is shown and the maximum peak is aligned at about 5ns. Region 13 is a typical LOS region where the first arriving component is very strong compared to all others.

In Section III, a geo-regioning algorithm is introduced which is based on the average power delay profiles (APDP) of the regions. The APDP of a Region A is determined by

$$\mathrm{APDP}_A(k) = \frac{1}{M_A} \sum_{m=1}^{M_A} |h_{A,m}(k)|^2, \qquad (1)$$

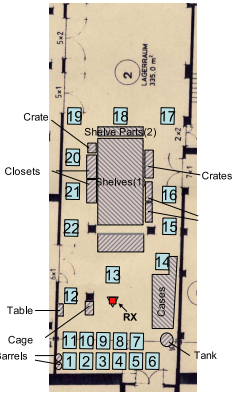

Fig. 1. Positions of RX array and wagon

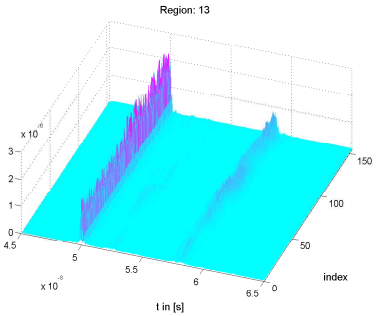

Fig. 2. Measured signatures from Region 13

where M_A is the number of available measurements of impulse responses or signatures from Region A represented by the sampled series $h_{A,m}(k)$. The m-th PDP of Region A is then $|h_{A,m}(k)|^2, k = 1...K$. In Fig. 3, the APDPs of two NLOS regions, Region 17 and 19, are shown. Both regions have almost the same distance to the receiver and are located almost symmetrically in the room (see Fig. 1). Although the APDPs look quite similar, significant differences which are indicated by the arrows can be observed. These considerations motivate the algorithm proposed in Section III.

III. A GEO-REGIONING ALGORITHM

We assume that the average power delay profiles (APDP) of all regions are a priori known at the receiver. This means that the receiver has a look up table (LUT) containing the APDPs of all regions that shall be distinguished. The main

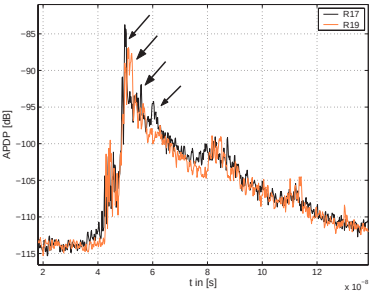

Fig. 3. APDPs of Regions 17 and 19

idea of our algorithm is that each APDP virtually provides a simple channel model for the impulse responses originating from the associated region. We assume a Gaussian distribution of the taps at each time instant k. Each signature $x(k)$, with $k = 1...K$, is an outcome of a random process that generates statistically independent Gaussian variables. The Gaussian distribution is zero mean and the variance at index k depends on the region where the signature originates from and is set to the corresponding APDP value:

$$\sigma^2(k) := \text{APDP}(k) \tag{2}$$

So, the probability density of $x(k)$ which is originating from Region A is $\mathcal{N}(0, \sigma_A^2(k))$:

$$p(x(k)|A) = \frac{1}{\sqrt{2\pi}\sigma_A(k)} \cdot \exp\left(-\frac{x^2(k)}{2\sigma_A^2}\right) \tag{3}$$

Here, the Gaussian assumption is applied for simplicity. However, recent investigations on the tap distributions in UWB channels support the Gaussian assumption [9]. There, it is also stated that the taps are correlated. Correlation is neglected in this paper. We will here derive the maximum a posteriori (MAP) detector considering the fact that only a very limited number of measurements M are available. That means that only an estimated version $\hat{\sigma}^2$ of the actual variance σ^2 is available at the receiver. The MAP approach maximizes the probability that the received signature $\vec{x}$ is an outcome of region $\mathcal{R}$ given the estimated variance $\hat{\sigma}^2_{\mathcal{R}}$ of region $\mathcal{R}$. Since the samples $x(k)$ are assumed to be statistically independent we simply investigate the scalar approach and neglect the index k for simpler notation:

$$\max_{\mathcal{R}} P(\mathcal{R}|x, \hat{\sigma}^2_{\mathcal{R}}) \tag{4}$$

With Bayes rule and statistical independency of x and $\hat{\sigma}^2_{\mathcal{R}}$ we get:

$$\begin{aligned} P(\mathcal{R}|x,\hat{\sigma}^2_{\mathcal{R}}) &= \frac{p(x,\hat{\sigma}^2_{\mathcal{R}}|\mathcal{R})\cdot P(\mathcal{R})}{p(x,\sigma^2_{\mathcal{R}})} \\ &\Rightarrow \frac{p(x,\hat{\sigma}^2_{\mathcal{R}}|\sigma^2_{\mathcal{R}})}{p(x,\hat{\sigma}^2_{\mathcal{R}})} \\ &= \frac{p(x|\sigma^2_{\mathcal{R}})\cdot p(\hat{\sigma}^2_{\mathcal{R}}|\sigma^2_{\mathcal{R}})}{p(x)\cdot p(\hat{\sigma}^2_{\mathcal{R}})} \end{aligned} \tag{5}$$

Here $P(\mathcal{R})$ is assumed to be equal for all regions. Again applying Bayes rule and cancelling the konstant term $p(x)$ we rewrite the result from (5):

$$p(x|\sigma^2_{\mathcal{R}})\cdot\frac{p(\sigma^2_{\mathcal{R}}|\hat{\sigma}^2_{\mathcal{R}})}{p(\sigma^2_{\mathcal{R}})} \tag{6}$$

The probability density function $p(\sigma^2_{\mathcal{R}}|\hat{\sigma}^2_{\mathcal{R}})$ can be given in terms of a Mth order χ^2-distribution:

$$\begin{aligned} p(\sigma^2_{\mathcal{R}}|\hat{\sigma}^2_{\mathcal{R}}) &= \frac{(M-1)\hat{\sigma}^2_{\mathcal{R}}}{\sigma^4_{\mathcal{R}}}\cdot p_{\chi_M}\left(\frac{(M-1)\hat{\sigma}^2_{\mathcal{R}}}{\sigma^2_{\mathcal{R}}}\right) \\ &= \frac{(M-1)\hat{\sigma}^2_{\mathcal{R}}}{\sigma^4_{\mathcal{R}}}\cdot\frac{\left[\frac{(M-1)\hat{\sigma}^2_{\mathcal{R}}}{\sigma^2_{\mathcal{R}}}\right]^{M/2-1}\cdot e^{-\frac{(M-1)\hat{\sigma}^2_{\mathcal{R}}}{2\sigma^2_{\mathcal{R}}}}}{2^{M/2}\cdot\Gamma(M/2)} \end{aligned} \tag{7}$$

To get rid of the unknown variable $\sigma^2_{\mathcal{R}}$ in (5) we remove it by integration:

$$\begin{aligned} &\int_0^\infty p(x|\sigma^2_{\mathcal{R}})\cdot\frac{p(\sigma^2_{\mathcal{R}}|\hat{\sigma}^2_{\mathcal{R}})}{p(\sigma^2_{\mathcal{R}})}p(\sigma^2_{\mathcal{R}})\,d\sigma^2_{\mathcal{R}} \\ &= \int_0^\infty p(x|\sigma^2_{\mathcal{R}})\cdot p(\sigma^2_{\mathcal{R}}|\hat{\sigma}^2_{\mathcal{R}})\,d\sigma^2_{\mathcal{R}} \end{aligned} \tag{8}$$

Substituting (7) and (3) into (8) leads to an integral which can be solved. The solution is:

$$\sigma^{M/2}_{\mathcal{R}}\cdot\left[\frac{x^2+(M-1)\hat{\sigma}^2_{\mathcal{R}}}{2}\right]^{-\frac{M+1}{2}}\cdot\Gamma\left(\frac{M+1}{2}\right) \tag{9}$$

If the same number M of measurements are available for all regions the term of the Γ-function is constant and can be neglected.

Below, we will compare the performance of this estimator with a simpler one which just assumes the estimated variance to be the actual one [1]. It considers all regions $\mathcal{R}$ and maximizes the probability density

$$\max_{\mathcal{R}} p(\vec{x}|\sigma^2_{\mathcal{R}}), \tag{10}$$

with $\vec{x}=\{x(k)\}, k=1...K$.

In case of only two hypotheses, regions A and B, this maximum likelihood estimator can be written as:

$$p(\vec{x}|A)\underset{B}{\overset{A}{\gtrless}}p(\vec{x}|B), \tag{11}$$

Since the samples $x(k)$ are assumed to be statistically independent we can simplify (11):

$$\sum_{k=1}^{K}x^2(k)\frac{\sigma^2_A(k)-\sigma^2_B(k)}{\sigma^2_A(k)\sigma^2_B(k)}\underset{B}{\overset{A}{\gtrless}}\sum_{k=1}^{K}\ln\frac{\sigma^2_A(k)}{\sigma^2_B(k)} \tag{12}$$

The right hand term is the decision threshold and is independent from the received signature. So, for each decision, only the simple sum on the left hand side has to be calculated.

In Fig. 4 and 5 the pairwise error probability for two regions A and B is shown. The results are achieved by simulations with Gaussian variables. The ratio σ^2_A/σ^2_B has been fixed and M observations of x for each region have been used to estimate the variance. Then, further observations have been used to simulate the pairwise error probability by applying the estimators in (9) and (12), respectively. Fig. 4 shows the

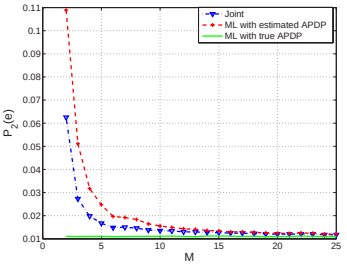

Fig. 4. Performance comparison of estimation for high ratio $\sigma^2_A/\sigma^2_B = 15000$

error probability for a very high ratio $\sigma^2_A/\sigma^2_B = 15000$. (In the next section we will show that the performance is determined by this ratio only.) We observe that for lower M the estimator from (9) achieves an improvement compared to the simpler one from (12). However, as shown in Fig. 5 for more realistic ratios the improvement vanishes and both estimators perform equally well. We conclude that for practical applications both estimators have similar performance. Therefore, we only consider the simpler one in the outline of the paper and do no longer distinguish between estimated and actual values of the variances.

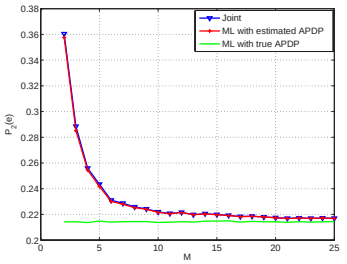

Fig. 5. Performance comparison of estimation for usual ratio $\sigma^2_A/\sigma^2_B = 15$

IV. On the error performance of two regions

A. Performance Measure and Simulations

The performance of the algorithm is shown by means of simulations running with the measured data. As a performance measure we use the pairwise error probability when deciding between two regions. We assume that we have received a noisy estimate $x(k), k = 1...K$ of the signature $\tilde{x}(k)$, where $n(k)$ denotes an additive zero mean Gaussian noise component with variance σ_n^2: $x(k) = \tilde{x}(k) + n(k)$. Hence, $x(k)$ is the sum of two Gaussian distributed random variables. If we assume $\tilde{x}(k)$ originating from Region A, the probability density function of $x(k)$ is $\mathcal{N}(0, \sigma_A^2(k) + \sigma_n^2)$. Accordingly, the variances in Eq. (12) have to be adapted: $\sigma_{A'}^2(k) = \sigma_A^2(k) + \sigma_n^2$. As performance measure the pairwise error probability, $P_2(e)$, is plotted over receive SNR. 150 signatures from one region and 150 from another region are taken from the measurements and added with white Gaussian noise with variance σ_n^2. The detector of (12) is applied and its error performance is evaluated. The SNR is defined by the mean received power per signature over the noise power:

$$\text{SNR} = \frac{1}{\sigma_n^2} \cdot \frac{1}{N_A + N_B} \sum_{m=1}^{N_A+N_B} \sum_{k=1}^{K} |h_m(k)|^2 \qquad (13)$$

B. Scalar Error Probability and Number of Taps

To get a better insight into the performance of the algorithm, we investigate the simple case of one single tap ($K = 1$). Then, the two hypotheses A and B correspond to two Gaussian distributions with zero mean and variances $\sigma_{A'}^2$ and $\sigma_{B'}^2$. If the error probability that an outcome x of Region B is detected as an outcome from Region A is written as $P_e(A|B)$ and vice versa as $P_e(B|A)$, the total error probability is:

$$P_2(e) = \frac{1}{2} P_e(A|B) + \frac{1}{2} P_e(B|A) \qquad (14)$$

It can be shown that $P_2(e)$ depends only on the ratio α of the two variances

$$\alpha := \frac{\sigma_{A'}^2}{\sigma_{B'}^2} \qquad (15)$$

and is given by:

$$P_2(e) = \frac{1}{2} + \frac{1}{2} \left[\text{erf}\left(\sqrt{\frac{\alpha \cdot \ln \alpha}{2(\alpha - 1)}} \right) - \text{erf}\left(\sqrt{\frac{\ln \alpha}{2(\alpha - 1)}} \right) \right] \qquad (16)$$

Fig. 6 shows a simulation result for the very similar regions 17 and 19 from Fig. 3. The K taps with maximum ratio α_0

$$\alpha_0 := \max \left\{ \frac{\sigma_{A'}^2}{\sigma_{B'}^2}, \frac{\sigma_{B'}^2}{\sigma_{A'}^2} \right\} \qquad (17)$$

are selected in this simulation for $K = 1, 30, 60, 300, 600$. The best performance is achieved for $K = 600$ taps. Decreasing K decreases the performance and an error floor can be observed. As expected $K = 1$ is not useful and yields $P_2(e) > 0.1$ in the considered SNR range. Note that this region pair is very crtical and that in general a much lower number of taps is required to achieve $P_2(e) < 10^{-2}$. A similar simulation with Gaussian distributed taps has been performed to investigate the impact of K on the performance, given the measured APDPs of several region pairs. The result is shown in Fig. 7. The lowest SNR (20dB) was set for the pair R03R13. The error floor appears already at $K \approx 30$. Both are LOS regions but the distance between R13 and RX is lower than between R03 and RX. Therefore, the received energy is higher for R13 and for lower K the performance improvement with k is very high. Normalizing the receive energy of the two regions shows that the improvement is less steep. Due to the higher SNR for this simulation (30dB) a much higher number of taps contribute until the error floor is reached. The weakest performance improvement with K achieve the two neighbor regions R02R03 whereas R17R18 improve remarkably steep.

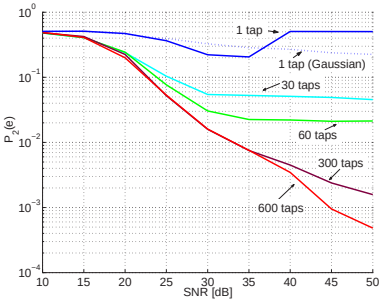

Fig. 6. Pairwise error probabilities for Regions 17 & 19 for various number of taps

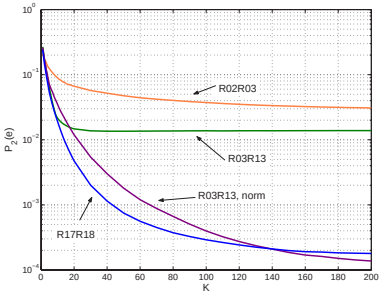

Fig. 7. Pairwise error probabilities over K for various regions (and various SNR)

In order to investigate the performance of the ML estimator more thoroughly, we focus in the next section V on an analytic approximation of the PEP, which provides statistical insight, a better understanding of the influence of system parameters

like region size and bandwidth, and the possibility to evaluate the regioning algorithm.

V. Approximation of the Pairwise Error Probability

Recalling again the ML estimator from (12) including noise at the receiver (13) gives

$$\sum_{k=1}^{K} x^2(k)\frac{\sigma^2_{A'}(k)-\sigma^2_{B'}(k)}{\sigma^2_{A'}(k)\sigma^2_{B'}(k)} \underset{B}{\overset{A}{\gtrless}} \sum_{k=1}^{K} \ln\frac{\sigma^2_{A'}(k)}{\sigma^2_{B'}(k)} \tag{18}$$

Introducing the RV Z as the log-likelihood decision variable and $\xi(k) = \text{sign}(\sigma^2_{A'}(k) - \sigma^2_{B'}(k))$ we get

$$Z = \sum_{k=1}^{K} \xi(k) Y^2(k) \underset{B}{\overset{A}{\gtrless}} \delta. \tag{19}$$

Each $Y(k)$ is a gaussian RV with zero mean and variance

$$\sigma^2_Y(k) = \sigma^2_X(k)\frac{|\sigma^2_{A'}(k)-\sigma^2_{B'}(k)|}{\sigma^2_{A'}(k)\sigma^2_{B'}(k)}. \tag{20}$$

Consequently, the RV $Y^2(k)$ is distributed according to a Gamma distribution with parameters $\rho = 0.5$ and $\beta(k) = 2\sigma^2_Y(k)$. The Gamma PDF with the two parameters ρ and β is given by

$$G(\rho,\beta) = \frac{z^{\rho-1}\exp(-z/\beta)}{\Gamma(\rho)\beta^\rho} \quad z \geq 0 \text{ and } \rho,\beta > 0 \tag{21}$$

with the characteristic function (CF) $\Phi(s) = (1-s\beta)^{-\rho}$.

A. Statistical Analysis of Z

The RV Z (c.f. (19)) is split into K_1 additive components ($\xi(k) = 1$) and $K - K_1$ subtractive components ($\xi(k) = -1$) according to

$$Z = Z_1 - Z_2 = \sum_{k=1}^{K_1} Y^2(k) - \sum_{k=K_1+1}^{K} Y^2(k), \tag{22}$$

where Z_1 and Z_2 are sums of independent gamma distributed RVs with constant ρ-parameters of 0.5 and varying β parameters.

Hereafter, the two RVs Z_1 and Z_2 are written as Z_q for $q \in \{1,2\}$. The following considerations hold for both RVs.

The cumulants $c_{n,q}$ of Z_q can be expressed in terms of the variances $\sigma^2_Y(k)$ (c.f. (20)) according to

$$\begin{aligned} c_{n,1} &= 2^{(n-1)}\cdot(n-1)!\sum_{k=1}^{K_1}(\sigma^2_Y(k))^n \\ c_{n,2} &= 2^{(n-1)}\cdot(n-1)!\sum_{k=K_1+1}^{K_2}(\sigma^2_Y(k))^n \end{aligned} \tag{23}$$

for Z_1 and Z_2, respectively.

It is not possible to find a mathematically tractable analytical expression for the PDFs of the RVs Z_q, but the parameters for an approximating Gamma (c.f. V-B) distribution can be determined through the cumulants given in (23).

B. Gamma Approximation

Since the summation of Gamma distributed RVs with identical β parameters is again a Gamma distributed RV, it is natural to use a Gamma distribution to approximate the PDFs of the RVs Z_q.

The approximation procedure for the PDF of Z is done in two steps. First the two RVs Z_q are approximated separately by two Gamma distributions and then these two PDFs are convolved to calculate the PEP.

The parameters ρ_q and β_q of the equivalent Gamma PDFs are chosen such that their means and variances correspond to the first two cumulants $c_{1,q}$ and $c_{2,q}$ (c.f. 23), i.e., the means and the variances, of the real distributions of the RVs Z_q:

$$\begin{aligned} \rho_q &= \frac{(c_{1,q})^2}{c_{2,q}} \\ \beta_q &= \frac{c_{2,q}}{c_{1,q}}. \end{aligned} \tag{24}$$

Consequently, the mean and the variance of the equivalent Gamma PDFs are given by

$$\begin{aligned} \mu_q &= \rho_q\beta_q = \frac{(c_{1,q})^2}{c_{2,q}}\cdot\frac{c_{2,q}}{c_{1,q}} = c_{1,q} \\ \sigma_q &= \rho_q(\beta_q)^2 = \frac{(c_{1,q})^2}{c_{2,q}}\cdot\left(\frac{c_{2,q}}{c_{1,q}}\right)^2 = c_{2,q}. \end{aligned} \tag{25}$$

An exemplary visualizations of the accuracy of the two presented approximations obtained from measured data [8] is given in Fig. 8, where the histogram is obtained from Monte Carlo simulations and serves as a reference.

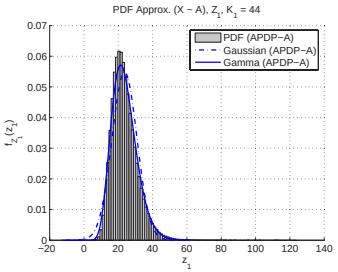

Fig. 8. PDF Approximations

In order to compute $P(Z = Z_1 - Z_2 \leq \delta)$, one has to evaluate the convolution integral

$$F_Z(\delta) = F_{Z_1}(-\delta) * F_{Z_2}(\delta) = \int_{-\infty}^{\infty} F_{Z_1}(\delta+\tau)F_{Z_2}(\tau)\mathrm{d}\tau, \tag{26}$$

where $F_{Z_1}(.)$ and $F_{Z_2}(.)$ are the corresponding cumulative distribution functions (CDFs) of $f_{Z_1}(.)$ and $f_{Z_2}(.)$, which are just Gamma PDFs with parameters found in (24).

C. Approximation Accuracy

In this section the accuracy of the introduced approximations to calculate the PEP is investigated. To judge whether the approximation is applicable, we use the relative approximation error criterion given by

$$E = \frac{P_2(e) - \hat{P}_2(e)}{P_2(e)}, \tag{27}$$

where $P_2(e)$ is the reference PEP (14) computed by Monte Carlo simulations with 10^6 samples, drawn from a normal distribution and processed according to the ML algorithm. The Monte Carlo results are considered to be reliable for a PEP $> 10^{-4}$, which is the area of interest for the UWB geo-regioning approach.

The geographical regions are represented by their APDPs $\sigma_A^2(k)$ and $\sigma_B^2(k)$, which are generated randomly according to a Gamma distribution with $\rho = 0.5$ and $\beta = 4$.

100 simulation runs for random APDPs with 80 taps and SNRs (c.f. (13)) between 0 and 25 dB are performed. Fig. 9 shows quantile plots for 80 APDP taps. This means that the 100 simulation runs are sorted according to ascending relative approximation error (27) at an SNR of 22 dB and the tenth (almost best case) and ninetieth (almost worst case) simulation runs are plotted.

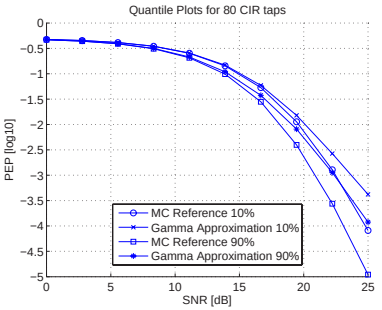

Fig. 9. PEP Approximation for 80 taps APDP

More results including also the Gaussian Approximation found from the central limit theorem are presented in Fig. 10. The regions are now represented by the ratios $\alpha(k) = \frac{\sigma_A^2(k)}{\sigma_B^2(k)}$, which are generated randomly according to a uniform distribution in the interval $[\frac{1}{20}, 20]$ and have the length 100. Here 1000 independent iterations are performed and the averaged PEPs are plotted over the SNR.

In this figure it is visible that the Gaussian Approximation performs worse than the Gamma Approximation except for high noise variances (i.e. high pairwise error probability), where they give roughly the same result, which matches the real pairwise error probability very well.

With this Gamma approximation it is possible to evaluate the ML detection algorithm instantaneously and get a rough idea on performance bounds or parameter variations. Additionally the approximation can also be used for a small number of CIR taps.

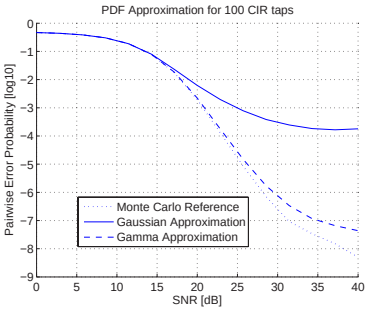

Fig. 10. PDF Approximation for 100 CIR taps

VI. Conclusions

We introduced the geo-regioning approach which makes use of the knowledge of the region's APDPs to localize UWB transmitters. We showed that in practical use a simple algorithm performs equally well as a more sophisticated one which considers the uncertainty in the APDP estimates. Discussing the impact of the number of available tap estimates we derived a criterion for tap selection which could be applied by a selective rake receiver. Further an approximation of the pairwise error probability has been derived which enables a thorough investigation of the geo-regioning performance by avoiding time consuming simulations.

References

[1] F. Althaus, F. Troesch, and A. Wittneben. UWB geo regioning in rich multipath environment. In *IEEE Vehicular Technology Conference, VTC Fall 2005*, September 2005.

[2] F. Althaus, F. Troesch, and A. Wittneben. Geo regioning in UWB networks. In *IST Mobile Summit, Dresden 2005*, June 2005.

[3] D. Porcino and W. Hirt. Ultra-wideband radio technology: Potential and challenges ahead. 41(7):66–74, July 2003.

[4] S. Gezici, Z. Tian, G. Giannakis, H. Kobayashi, A. Molisch, H. Poor, and Z. Sahinoglu. Localization via ultra-wideband radios. *IEEE Signal Processing Magazine*, pages 70–84, July 2005.

[5] Joon-Yong Lee and Robert A. Scholtz. Ranging in a dense multipath environment using an UWB radio link. In *IEEE Journal on Selected Areas in Communications, Vol. 20, No.9*, pages 1677–1683, December 2002.

[6] S. J. Ingram, D. Harmer, and M. Quinlan. Ultra wideband indoor positioning systems and their use in emergencies. In *Position Location and Navigation Symposium*, pages 706 – 715, April 2004.

[7] D. Niculescu. Positioning in ad hoc sensor networks. In *Network, IEEE*, pages 24 – 29, July/August 2004.

[8] F. Althaus, F. Trösch, T. Zasowski, and A. Wittneben. Sts measurements and characterization. *PULSERS Deliverable D3b6a*, IST-2001-32710 PULSERS, 2005.

[9] Ulrich G. Schuster and Helmut Bölcskei. Ultra-wideband channel modeling on the basis of information-theoretic criteria. *IEEE Journal on Selected Areas in Communications*, mar 2005.